


Recombinant Human Heavy Chain Ferritin Nanoparticles Serve as ROS Scavengers for the Treatment of Ischemic Stroke

Mi Qi , Yajuan Cheng, Ke Liu, Jingxing Cai, Tianyu Liu, Xiaoying Wu, Huili Tang, He Huang, Qinbiao Chen, Xiaoguang Zhou

The Eighth Affiliated Hospital, Sun Yat-sen University, Shenzhen, Guangdong, People's Republic of China

Correspondence: Mi Qi; Xiaoguang Zhou, Tel +86-13510794978; +86-18818780760, Email qimi@mail.sysu.edu.cn; gzzhouxg@163.com

Purpose: Ischemic stroke is a high-incidence disease that threatens human well-being. The potent neuroprotective effects render reactive oxygen species (ROS) scavengers potential agents for acute ischemic stroke therapy. Challenges such as inadequate permeability across the blood-brain barrier (BBB), limited half-life, and adverse effects hinder the widespread utilization of small molecule and inorganic ROS scavengers. Thus, there is an urgent demand for efficacious neuroprotective agents targeting ischemic stroke. Our study discovered the superoxide dismutase (SOD)-mimetic activity of recombinant human heavy chain ferritin (rHF) nanoparticles expressed from *Escherichia coli* (*E. coli*). Subsequent investigations delved into the ROS-scavenging proficiency of rHF within neural cells, its therapeutic efficacy against ischemic stroke, and the elucidation of its neuroprotective mechanisms.

Methods: rHF protein nanoparticles were expressed in *E. coli* and purified *via* size-exclusion chromatography. The superoxide anion ($\bullet\text{O}_2^-$) scavenging SOD-mimetic activity of rHF nanoparticles was measured using a SOD detection kit. The ROS scavenging ability and protection effects against oxidative damage of rHF nanoparticles were studied in H_2O_2 -induced PC12 cells. Therapeutic effects and neuroprotective mechanisms of rHF against ischemic stroke were investigated with transient middle cerebral artery occlusion (MCAO) reperfusion mice model.

Results: rHF nanoparticles can eliminate excessive ROS in nerve cells and alleviate oxidative damage. The results of animal experiments demonstrated that rHF nanoparticles passed across BBB, reduced infarct areas in brain tissue, and lowered the neurological deficit score of ischemia-reperfusion model mice. Additionally, rHF nanoparticles mitigated neuronal apoptosis and ferroptosis, suppressed microglial activation, maintained oxygen homeostasis, and exhibited negligible organ toxicity.

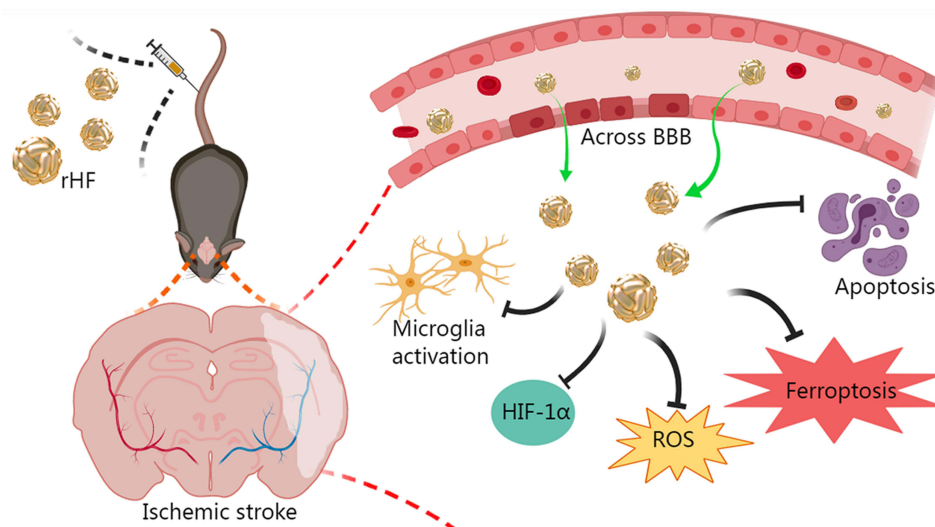
Conclusion: rHF nanoparticle could be developed as a new ROS scavenger for nerve cells and has therapeutic potential as a drug for cerebral ischemia-reperfusion injury.

Keywords: human heavy chain ferritin, ROS scavenger, ischemic stroke, SOD-mimetic, neuroprotection

Introduction

Stroke is the second-leading cause of death and the third-leading cause of death and disability globally, and the incidence has increased continually in the past 30 years.¹ Ischemic stroke, accounting for almost 80% of all strokes, causes a constant medical burden to society.² Currently, the methods for ischemic stroke treatment include thrombolysis, thrombectomy, and neuroprotective therapies to restore cerebral blood flow and protect brain function.^{3,4} Nonetheless, owing to the constrained therapeutic time window of 4.5 hours following the onset of stroke, only a minority of patients can avail themselves of timely and effective thrombolytic therapy.⁵ In addition, the efficacy of these treatments is restricted by secondary damages mainly caused by oxidative stress, excitotoxicity, apoptosis, and neuroinflammation.^{6,7} Reperfusion after thrombolytic therapy causes excessive production of harmful reactive oxygen species (ROS), such as superoxide anion radicals ($\bullet\text{O}_2^-$), hydroxyl radicals ($\bullet\text{OH}$), hydrogen peroxide (H_2O_2), and nitric oxide (NO), leading to increased neuronal death through protein oxidation, DNA damage, and lipid peroxidation.⁸ Thus, ROS scavenging-based neuroprotective therapy becomes

Graphical Abstract



a leading strategy for ischemic stroke treatment. The application of small molecule radical scavengers (such as edaravone,⁹ DI-3-n-Butylphthalide,¹⁰ and atorvastatin¹¹) and nano-antioxidants (such as CeO₂ nanoparticles,^{12–14} melanin,¹⁵ carbon dot,¹⁶ platinum,¹⁷ and manganese dioxide^{18,19}) have been proven as promising approaches for efficient treatments for stroke. Nevertheless, the clinical utilization of small-molecule ROS scavengers or nano-antioxidants is hampered by their abbreviated half-life, limited bioavailability, inadequate permeation across the blood-brain barrier (BBB), and potential off-target side effects.²⁰ Hence, the imperative need arises for the development of agents possessing robust ROS scavenging activity and favorable physicochemical properties to address the treatment of ischemic stroke.

Ferritin is a cage-like protein nanoparticle that binds and stores iron in various organisms. Recombinant human heavy chain ferritin (rHF) can be self-assembled from 24 subunits to form protein cages in vitro with an outer diameter of 12 nm and an inner cavity of 8 nm.²¹ rHF can encapsulate many inorganic particles and small molecule drugs, making it a widely used drug delivery carrier.^{22,23} Furthermore, rHF exhibits the ability to traverse the BBB by binding to mouse T-cell immunoglobulin mucin receptor 2 (TIM-2) or human transferrin receptor 1 (TfR1), both of which are prominently expressed in the endothelial cells of the BBB. This characteristic endows rHF with inherent nanocarrier properties for efficient transport across the BBB.^{24–27} Moreover, heavy chain ferritin exerts inhibition on tumor necrosis factor (TNF)-induced apoptosis by mitigating the accumulation of reactive oxygen species (ROS)²⁸ and diminishing iron-dependent ferroptosis through the chelation of excessive iron ions.^{29,30} These findings suggest that rHF is a potential agent for treating ROS-related brain diseases, such as ischemic stroke, Alzheimer's disease (AD), and Parkinson's disease (PD). Nonetheless, while rHF has previously been employed solely as a carrier for brain-targeted drug delivery,^{24,27} its inherent neuroprotective properties and therapeutic effects on ischemic stroke remain unexplored.

The current study showcased the superoxide dismutase (SOD) mimetic activity of rHF nanoparticles purified from *Escherichia coli* (*E. coli*). Subsequently, we investigated the in vitro ROS-scavenging capacity of rHF and its therapeutic effectiveness in mitigating ischemic stroke using an ischemia-reperfusion mice model. The results showed that rHF nanoparticles exhibit effective ROS scavenging ability and protect PC12 neuronal cells from free radical-induced oxidative damage. Furthermore, rHF nanoparticles demonstrate the ability to traverse the BBB, leading to reduced infarct areas, inhibition of neuronal apoptosis and ferroptosis within brain tissue, and suppression of microglial activation. These findings collectively underscore the promising efficacy of rHF nanoparticles in neuroprotective therapy for ischemic stroke. Taken together, rHF nanoparticles offer a novel therapeutic strategy for neuroprotection and prevent the injury induced by reperfusion in ischemic stroke.

Materials and Methods

Materials

2–6 nm cerium oxide (CeO₂) nanoparticles were purchased from Nanjing XFNANO Materials Tech Co., Ltd (Nanjing, China). PD-10 SephadexTM G-25 columns were from Cytiva (Buckinghamshire, UK). Anti-B-cell lymphoma-2 (Bcl-2) rabbit polyclonal antibody, anti-ionized calcium-binding adaptor molecule-1 (Iba-1) rabbit polyclonal antibody, anti-glutathione peroxidase 4 (GPX4) rabbit polyclonal antibody, and fluorescein isothiocyanate (FITC) TUNEL Cell Apoptosis Detection Kit were from Servicebio (Wuhan, China). Anti-hypoxia-inducible factor 1 α (HIF-1 α) rabbit polyclonal antibody was bought from XY-Bioscience (Shanghai, China). SOD Assay Kit was from Dojindo Laboratories (Kumamoto, Japan). H2DCFDA (DCFH-DA) was purchased from UELandy Inc. (Suzhou, China). PC12 cell line was obtained from iCell (Shanghai, China) and bEnd.3 cell line was from the BeNa Culture Collection (Beijing, China). RPMI-1640 medium, Dulbecco's modified Eagle's medium (DMEM), and fetal bovine serum (FBS) were procured from Gibco/Life Technologies (New York, USA).

Expression and Purification of rHF Protein

The construction of rHF expression vector and protein purification was conducted according to the previously reported method.²¹ In summary, the sequence encoding rHF (Gene ID: 2495) was inserted into the plasmid pET28a using the NdeI and XhoI restriction enzyme sites. This configuration ensured that the 6 \times His tag present in the plasmid would be fused to the amino terminus of the expressed rHF protein. The recombinant plasmid (pET28a-rHF) was transformed into *E. coli* cells of the Rosetta (DE3) strain and positive clones were cultured in Luria-Bertani (LB) medium with 50 μ g/mL kanamycin and 34 μ g/mL chloramphenicol at 37 °C until the OD₆₀₀ reached approximately 0.5. Then, rHF protein expression was induced with 1 mM isopropyl- β -D-thiogalactoside (IPTG), and cells were cultured at 20 °C for an additional 18 h under constant shaking. After incubation, the cells were collected by centrifugation (5000 g, 10 min), and cell pellets were resuspended in assembly buffer (20 mM Tris-HCl, 50 mM NaCl, pH 8.0) for sonication on ice for 40 min. The lysate was heated at 70 °C for 20 min, followed by centrifugation at 10,000 g at 4 °C for 40 min to precipitate the proteins. The supernatant was filtered using a 0.22- μ m filter and subjected to size-exclusion chromatography (GE Healthcare, Uppsala, Sweden) on a Superose 6 column to purify the rHF protein. The endotoxin in purified protein was removed using an EtEraserTM endotoxin removal kit (BIOENDO, Xiamen, China). Subsequently, the protein was concentrated by ultrafiltration (MW cutoff 100 kDa, Merck Millipore, Germany). The concentration of purified protein was determined using a BCA protein assay kit (Beyotime, Shanghai, China), according to the manufacturer's instructions.

Characterization of rHF Nanoparticles

The purified rHF protein was verified by sodium dodecyl sulfate-polyacrylamide gel electrophoresis (SDS-PAGE). The hydrodynamic size of rHF nanoparticles in the assembly buffer was determined based on dynamic light scattering (DLS), and zeta potential was measured based on phase analysis light scattering (PALS) on NanoBrook 90Plus PALS (Brookhaven, USA). DMEM or DMEM with 10% FBS was used to simulate blood plasma in vitro. The rHF nanoparticles were dissolved in DMEM or DMEM with 10% FBS for 2 or 3 days, and the stability of rHF nanoparticles was evaluated by testing hydrodynamic size based on DLS. The protein cages were also characterized using transmission electron microscopy (TEM). Briefly, a drop of rHF nanoparticles containing 0.5 mg/mL protein was placed onto a carbon-coated copper grid and stained with 2% phosphotungstic acid (pH 7.4). The dried grids were observed using a 200 kV field-emission transmission electron microscope (JEM-2100F, JEOL Ltd, Japan), and images were further analyzed using Image J software.

Evaluation of the SOD Mimetic Activity of rHF Nanoparticle

The superoxide anion (\bullet O₂⁻) scavenging activity of rHF nanoparticles was assessed based on the SOD inhibition rate with a commercially available SOD detection kit (Dojindo Laboratories, Japan). The steps were as follows: Step 1, 20 μ L rHF solution of different concentrations (0.03, 0.06, 0.13, 0.25, 0.5, 1, 2, and 4 mg/mL) was added into the sample well of a 96-well plate, and 20 μ L rHF solution of 4 mg/mL was added into blank 2 wells, respectively. Instead, 20 μ L of deionized water was

added into blank 1 and blank 3 wells, respectively. Step 2, 200 μL WST working solution was added into each well. In step 3, 20 μL of dilution buffer was added into blank 2 and blank 3 wells, while 20 μL of enzyme solution was added into the sample and blank 1 wells. In step 4, the plate was incubated at 37 $^{\circ}\text{C}$ for 20 min, and OD_{450} was recorded on a microplate reader (Model 680, Bio-Rad, USA). The inhibition rate of SOD was calculated according to the following formula: The Inhibition Rate of SOD (%) = $[(A_{\text{blank1}} - A_{\text{blank3}}) - (A_{\text{sample}} - A_{\text{blank2}})] / (A_{\text{blank1}} - A_{\text{blank3}}) \times 100$ (A_{sample} , A_{blank1} , A_{blank2} , and A_{blank3} represent the OD_{450} of sample, blank1, blank2, and blank3, respectively)

Evaluation of Cytotoxicity and Protection of PC12 Cells with rHF Against H_2O_2 -Induced Oxidative Damage

The cytotoxicity of rHF nanoparticles in the PC12 cell line was detected by the cell counting kit-8 (CCK-8) assay. Briefly, cells in RPMI 1640 with 10% FBS were seeded in 96-well plates at a density of 10^4 cells/well and incubated for 12 h to allow cell attachment. Then, the cells were treated with rHF at final concentrations of 3.125, 6.25, 12.5, 25, 50, 100, 200, and 400 $\mu\text{g}/\text{mL}$, respectively. An equal volume of phosphate-buffered saline (PBS) was used to treat the control group. After 24 h of incubation, the medium was removed and 110 μL of medium containing 10 μL of CCK-8 reagent was added to each well and incubated for an additional 4 h. Subsequently, OD_{450} was measured, and the relative cell viability was calculated using the following formula: Relative Cell Viability (%) = $(A_{\text{sample}} - A_{\text{blank}}) / (A_{\text{control}} - A_{\text{blank}}) \times 100$ (A_{sample} represents the OD_{450} of a well with cells, CCK-8 reagent, and sample solution, A_{control} represents the OD_{450} of the control well with cells and CCK-8 reagent, without substance solution, and A_{blank} represents the OD_{450} of the well with medium and CCK-8 reagent, without cells).

CCK-8 assay was also used to detect the reverse damage of rHF on PC12 cells induced by H_2O_2 . Briefly, PC12 cells (10^4 cells/well) were seeded in 96-well plates. After cell adherence, a mixture of H_2O_2 (500 μM) and various concentrations of rHF was added to each well and incubated for another 24 h before determining the cell viability by CCK-8 assay.

ROS Scavenging Ability of rHF Nanoparticles in PC12 Cell Line

PC12 cells were seeded in 96-well plates at a density of 2×10^4 cells/well and incubated for 12 h to allow cell adhesion. Then, the cells were pre-stained with 10 μM of ROS probe DCFH-DA for 30 min and incubated with H_2O_2 (500 μM) and different concentrations of rHF nanoparticles (0, 12.5, 25, 50, 100, 200, and 400 $\mu\text{g}/\text{mL}$) for 2 h. Additionally, the blank control group was devoid of both H_2O_2 and drugs, while all other experimental conditions remained consistent with those of the experimental group. The cells were analyzed for ROS generation after 2 h on a cell imaging multimode reader at excitation and emission wavelengths of 488 and 528 nm, respectively. The ROS was calculated using the following formula: % of Control = $E_{\text{sample}} / E_{\text{control}} \times 100$. Subsequently, the cells were fixed with 4% paraformaldehyde and photographed by light microscopy.

Labeling rHF Nanoparticles with Cy5.5

For fluorescence imaging, Cy5.5 was used to label rHF protein nanoparticles. Cy5.5 N-hydroxysuccinimide (NHS) ester (Cy5.5 NHS ester, GE Healthcare, USA) was incubated with rHF nanoparticles in sodium bicarbonate (0.1 M, pH 8.5) at the molar ratio of 10 Cy5.5 per rHF nanoparticle for 12 h. Subsequently, the mixture was purified on PD-10 SephadexTM G-25 columns in PBS at pH 7.4 to remove free Cy5.5 dye and concentrated by ultrafiltration (MW cutoff 100 kDa, Millipore, Germany).

In vitro Endocytosis Assay

PC12 or bEnd.3 cells (10^5 cells/well) were seeded in confocal dishes and incubated for 12 h. After cell adherence, 25 $\mu\text{g}/\text{mL}$ of Cy5.5-rHF nanoparticles were added, while the negative control group was treated with an equal volume of PBS. After incubation for 2 h, the cells were fixed with 4% paraformaldehyde and stained with 4',6-diamidino-2-phenylindole (DAPI). The cell fluorescence of Cy5.5 (Ex 673 nm/Em 707 nm) and DAPI (Ex 358 nm/Em 461 nm) was analyzed by Zeiss LSM 880 confocal microscopy.

In vitro BBB Transcytosis Assay

Mouse brain microvascular endothelial bEnd.3 cell line was used to establish an in vitro BBB model by transwell assay. Briefly, 5×10^4 bEnd.3 cells were seeded in the upper chambers (3 μm , Corning, USA) and incubated for several days until the trans-endothelial electrical resistance reached 200 $\text{ohm}\cdot\text{cm}^2$. Then, the PC12 cells were cultured in the lower chambers at a density of 5×10^4 cells/well. After cell adherence, different concentrations of Cy5.5-labeled rHF nanoparticles (25, 50, and 100 $\mu\text{g}/\text{mL}$) were added in the upper chambers for 24-h incubation. Subsequently, PC12 cells were fixed with 4% paraformaldehyde and stained with DAPI. Finally, the internalization of Cy5.5-rHF in PC12 cells was observed by fluorescence microscopy using excitation at 673 nm and emission at 707 nm.

In vivo Animal Experiments

Male C57BL/6 mice (4–6-weeks-old) were purchased from Zhuhai BesTest Bio-Tech Co., Ltd (Zhuhai, China). All animal experiments were performed in Shenzhen TOP Biotech Co., Ltd (Shenzhen, China) in compliance with the guidelines established by the Chinese Institutional Animal Care and Use Committee with the approval of the Animal Ethics Committee in the Eighth Affiliated Hospital of Sun Yat-sen University (2023-029-01). The transient middle cerebral artery occlusion (MCAO) mice model was established to evaluate the protective effects of rHF treatment against ischemia-reperfusion after stroke. In brief, the MCAO mice model was induced by inserting a filament with a silicone tip into the carotid bifurcation along the internal carotid artery, up to the origin of the middle cerebral artery, for 30 minutes. Subsequently, the filament was withdrawn to allow reperfusion. Conversely, the sham operation group underwent a procedure akin to the MCAO model, excluding silicone filament embolization. The MCAO model mice were randomly divided into saline and rHF (10, 20, and 30 mg/kg) treatment groups. After reperfusion, the samples were dispersed in 200 μL saline and immediately injected at the caudal vein. The neurological scores of MCAO mice after treatment were determined within 2 days using a Zea-Longa scoring system. Subsequently, the brain tissues were separated and washed with saline before slicing into six 2-mm sections. These brain slices were stained with 2% of 2,3,5-triphenyltetrazole chloride (TTC), followed by fixing in 4% paraformaldehyde for imaging and quantification. Then, brain sections were embedded in paraffin, sectioned, and processed for hematoxylin and eosin (H&E) staining, Nissl staining, and deoxynucleotidyl transferase-mediated deoxyuridine triphosphate nick-end labeling (TUNEL) Hoechst costaining. The expression levels of Bcl-2, GPX4, HIF-1 α , and Iba-1 (a marker of microglia) in brain sections were examined by immunofluorescence (IF) staining. The internalization of rHF in the brain tissue of MCAO model mice was additionally assessed through immunofluorescence staining (IF) utilizing an Alexa Fluor 488 anti-6 \times His tag monoclonal antibody (Abcam, UK), known for its specific binding to 6 \times His tag labeled rHF.

Toxicity Evaluation of rHF in vivo

Two days post-treatment, hearts, livers, spleens, lungs, and kidneys were collected from both Sham and MCAO mice and fixed in 4% paraformaldehyde. Subsequently, the organs were embedded in paraffin, sectioned, and subjected to H&E staining. Images of the H&E-stained sections were captured using a Nikon Ni-E camera (Nikon, Minato, Japan). Additionally, blood indicators of organ dysfunction, including blood urea, creatinine, alanine aminotransferase (ALT), and aspartate aminotransferase (AST), were assessed.

Statistical Analysis

Data are presented as the mean \pm standard deviation (SD). Multiple groups were compared using one-way analysis of variance (ANOVA), followed by Bonferroni's multiple comparisons. The results between the two groups were compared by unpaired *t*-test using GraphPad Prism. Differences of $*P < 0.05$, $**P < 0.01$, and $***P < 0.001$ were considered statistically significant.

Results and Discussion

Purification and characterization of rHF protein nanoparticles

The rHF protein was expressed in *E. coli*, purified via size-exclusion chromatography, and concentrated by ultrafiltration. SDS-PAGE displayed a major band of purified rHF with a molecular mass of approximately 20 kDa (Figure 1a), which is in accordance with the reported molecular mass of 21 kDa.²¹ The TEM images verified homogenous spherical cage-like structures of rHF nanoparticles (Figure 1b). The DLS results indicate a single distribution of rHF nanoparticles with an average diameter of 10.87 ± 0.8 nm (Figure 1c). The zeta potential of rHF nanoparticles in the assembly buffer was -11.73 ± 1.05 mV (Figure S1). The stability of rHF nanoparticles in vitro was assessed in DMEM or DMEM supplemented with 10% fetal bovine serum (FBS), which simulates blood plasma. As depicted in Figure S2, following incubation of rHF nanoparticles with DMEM or DMEM supplemented with 10% FBS for 2 or 3 days, there was no significant alteration in the hydrodynamic size of rHF. This observation suggests that rHF nanoparticles may maintain stability in blood plasma.

rHF Nanoparticles Have SOD Mimetic Activity in vitro

The superoxide anion ($\cdot\text{O}_2^-$) scavenging SOD-mimetic activity of rHF nanoparticles was measured using a SOD detection kit. Figure 1d demonstrates that rHF nanoparticles exhibit inhibition of WST-1 in a manner comparable to the activity of the SOD enzyme, with a 50% inhibitory concentration (IC_{50}) of 0.82 mg/mL. The response of rHF to scavenging $\cdot\text{O}_2^-$ is shown in Figure 1e. The SOD enzyme functions by scavenging ROS and mitigating oxidative damage within cells.³¹ It has been reported that the ferritin heavy chain displays ferroxidase activity and attenuates the induction of ROS and apoptosis through the sequestration of iron.^{28,32} Additionally, ferritin heavy chain-mediated iron depletion facilitates the disposal of H_2O_2 catalases and peroxidases, thereby impeding the formation of highly reactive hydroxyl radicals ($\cdot\text{OH}$).³³ The combined SOD-mimetic activity and ferroxidase activity of rHF may render it suitable for effectively removing excessive ROS within cells.

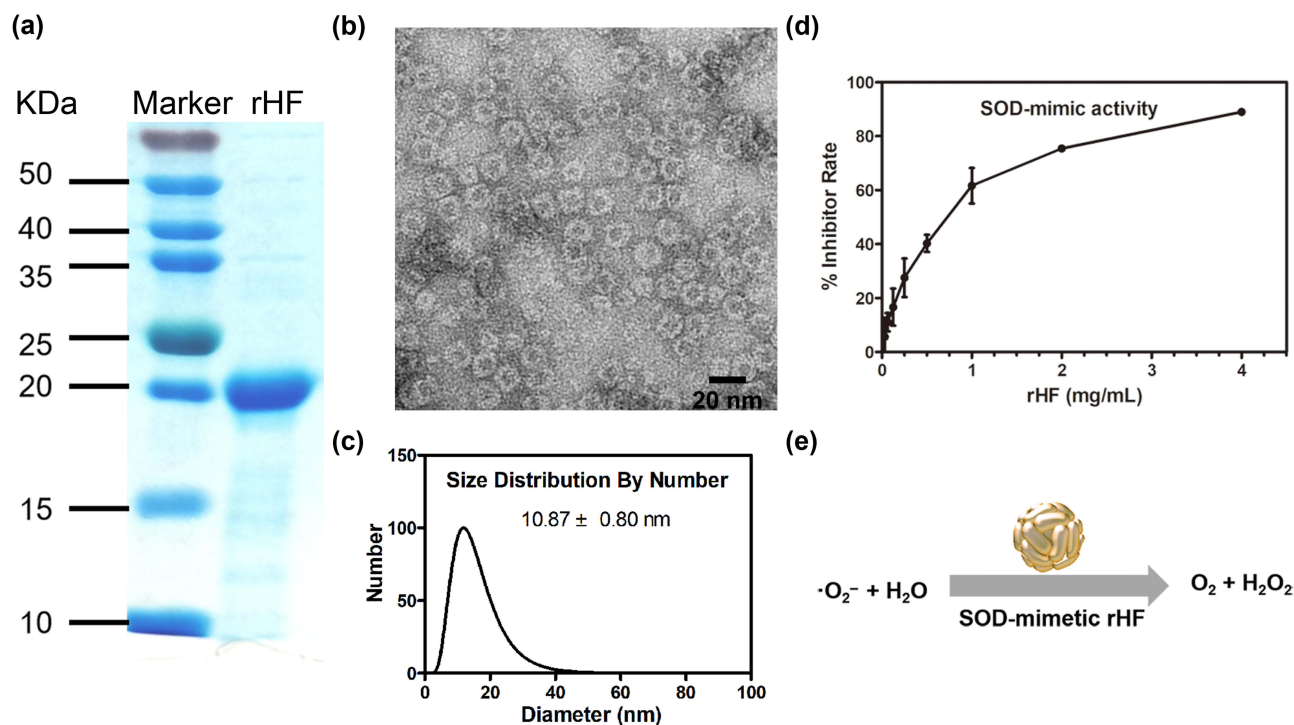


Figure 1 Purification and characterization of rHF nanoparticles. (a) SDS-PAGE analysis of the purified rHF monomer protein. The molecular mass of rHF is 21 kDa. (b) TEM images of rHF nanoparticles. Scale bar = 20 nm. (c) Size distribution of rHF nanoparticles analyzed via DLS. (d) Evaluation of superoxide anion ($\cdot\text{O}_2^-$) scavenging activity of rHF nanoparticles via SOD inhibition rate, IC_{50} : 0.82 mg/mL. (e) Schematic illustration of SOD mimetic rHF for scavenging $\cdot\text{O}_2^-$.

Cytotoxicity and ROS Scavenging Effects of rHF Nanoparticles in PC12 Cells

The rat adrenal medulla pheochromocytoma PC12 cell line possesses general characteristics of neuroendocrine cells, making it a widely utilized model in the fields of neuropharmacology and neurophysiology research.¹³ Therefore, PC12 cells damaged by ROS oxidation comprised the cell model for ischemic injury in stroke to evaluate the protective effect of rHF on PC12 cells against H₂O₂-induced oxidative damage. Initially, the cytotoxicity of rHF nanoparticles in PC12 cells was evaluated following a 24-hour co-incubation period. As shown in Figure 2a, different concentrations of rHF exhibited no cytotoxicity to PC12 cells. Also, the ability of rHF nanoparticles to enter PC12 cells was evaluated. Fluorescent images showed that Cy5.5-labeled rHF enter PC12 cells and are presented in the cytoplasm (Figure 2b).

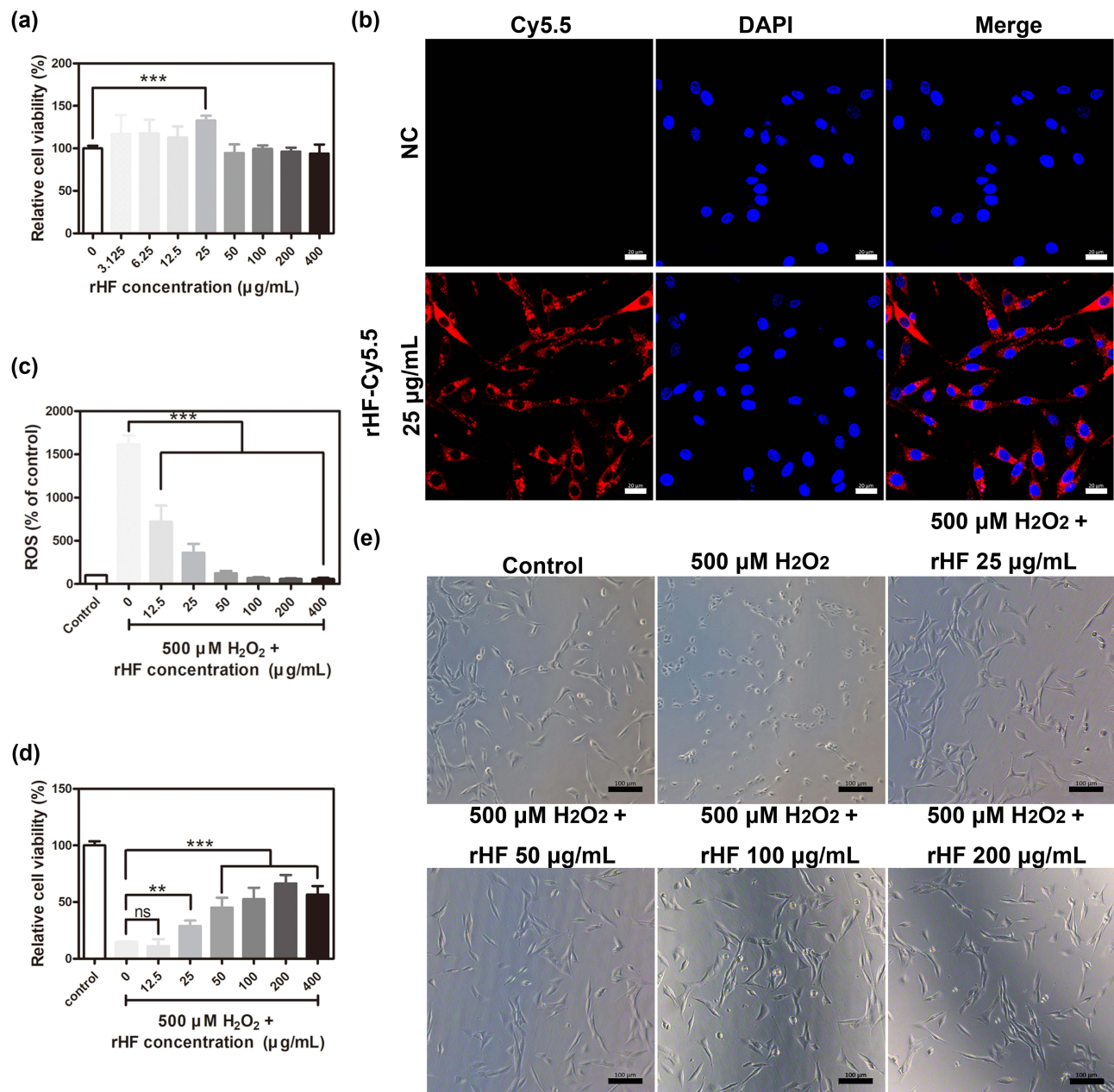


Figure 2 Cytotoxicity and ROS scavenging effects of rHF nanoparticles in PC12 cells. (a) Relative cell viability of PC12 cells following treatment with different concentrations of rHF nanoparticles for 24 h (n = 4). (b) Representative fluorescent image of Cy5.5-labeled rHF in PC12 cells, Scale bar = 20 µm. (c) Relative ROS in PC12 cells after treatment with H₂O₂ (500 µM) and various concentrations of rHF for 2 h (n = 4). (d) Relative cell viability of PC12 cells post-treatment with H₂O₂ (500 µM) and different concentrations of rHF for 24 h (n = 4). (e) Representative images of PC12 cells post-treatment with H₂O₂ (500 µM) and various concentrations of rHF for 2 h, Scale bar = 100 µm. **P < 0.01, ***P < 0.001, and ns indicates no significant difference.

Exposure to 500 μM of H_2O_2 induced a substantial increase in ROS levels in PC12 cells, leading to significant inhibition of cell viability and alteration of cell morphology from polygonal to round. Nevertheless, rHF effectively scavenged intracellular ROS, thereby reducing oxidative damage and inhibiting H_2O_2 -induced cell morphological changes in a dose-dependent manner (Figure 2c–e). In addition, we compared the ROS scavenging ability and protection against oxidative damage of rHF with the CeO_2 ROS scavenger. The results demonstrated that 20 $\mu\text{g}/\text{mL}$ of CeO_2 cannot reverse the ROS increase and 500 μM H_2O_2 -induced cell damage, while an equivalent dose of rHF exhibited superior performance (Figure S3).

Penetrative Capacity of rHF Nanoparticle Across BBB

The BBB serves as a barrier that restricts the exchange of molecules between the central nervous system and peripheral blood circulation. Consequently, traversing the BBB is imperative for effective drug delivery aimed at treating cerebral ischemic stroke. In this study, cellular uptake of Cy5.5-labeled rHF by brain microvascular endothelial bEnd.3 cell line, the main component of BBB, was investigated by confocal microscopy. Fluorescence images revealed that Cy5.5-labeled rHF penetrates bEnd.3 cells and exists in the cytoplasm (Figure 3a). We also performed a transwell assay for the coculture of bEnd.3 and PC12 cells to simulate the BBB model and evaluated the permeability of Cy5.5-labeled rHF (Figure 3b). As shown in Figure 3c, rHF is transported across the bEnd.3 cells after 24-h incubation and was taken up by PC12 cells in the lower chamber. After cerebral ischemia-reperfusion, BBB is disrupted and opens transiently.³⁴ Only a limited proportion of nanoparticles gain access to the brain lesion through the compromised BBB area. rHF can traverse the BBB via mouse TIM-2 or human TfR1 receptor-mediated transcytosis.²⁶ Hence, the permeability of rHF across the BBB will augment its accumulation in the brain lesion for stroke therapy. The internalization of rHF in the brain tissue of MCAO mice models following intravenous injection was investigated via immunofluorescence (IF) staining. Fluorescent images revealed the entry of rHF into the brain tissue, where it was taken up by nerve cells (Figure S4).

Therapeutic and Neuroprotective Effects of rHF Against Ischemia-Reperfusion in vivo

To investigate the therapeutic efficacy of rHF nanoparticles in vivo, the MCAO mice model was employed to simulate ischemia-reperfusion injury following stroke. Subsequently, MCAO mice were administered rHF via tail vein injection after the reperfusion procedure. The neurological deficit scores of the MCAO mice were evaluated for 2 days following the treatment. 48 h post-reperfusion, the brain tissues were sliced, and cerebral infarct volumes were measured by TTC staining, showing red in the stained normal regions and white in the infarction areas. The entire schedule of the mouse experiments is presented in Figure 4a. The results showed that the infarct volume in the saline group was approximately $32.9 \pm 12.8\%$, while the brain infarct area of rHF-treated mice significantly decreased in a dose-dependent manner. The infarct volumes decreased to $\sim 8.4 \pm 3.1\%$ at an optimal concentration of 30 mg/kg of rHF (Figures 4b, c and S5). The neurological deficit scores of MCAO mice after rHF (30 mg/kg) treatment also decreased significantly from 2.3 to 1.0 (Figure 4d).

Additionally, the neuroprotective effect of rHF was further investigated through pathological analysis of the brain tissue. Firstly, H&E staining of the brain sections in MCAO mice treated with saline displayed massive necrosis at the infarction site. In contrast, rHF (30 mg/kg) treatment decreased the area of necrosis (Figure 5a, top panel). Then, neuronal damage in the infarcted area of MCAO mice was examined by Nissl staining. The results revealed a significant decrease in the number of intact neurons within the infarcted area of MCAO mice treated with saline, as compared to the sham-operated control group. Moreover, the intact neurons exhibited irregular morphology and disordered arrangement. However, after treatment with rHF (30 mg/kg) for 2 days, the neuron damage in brain tissue decreased apparently (Figure 5a, middle panel).

Moreover, a TUNEL-Hoechst costaining assay was performed to investigate neuronal apoptosis within the infarcted area. The results revealed typical apoptotic features in the infarcted area of MCAO mice in the saline-treated group, whereas the rHF (30 mg/kg)-treated group showed reduced apoptosis of neurons (Figure 5a, bottom panel). The expression levels of Bcl-2, suppressing apoptosis in infarcted areas, were examined by IF staining. Compared to the saline group, the expression levels of Bcl-2 were much higher in the rHF group and were similar to those in the sham group (Figures 5b, d and S6).

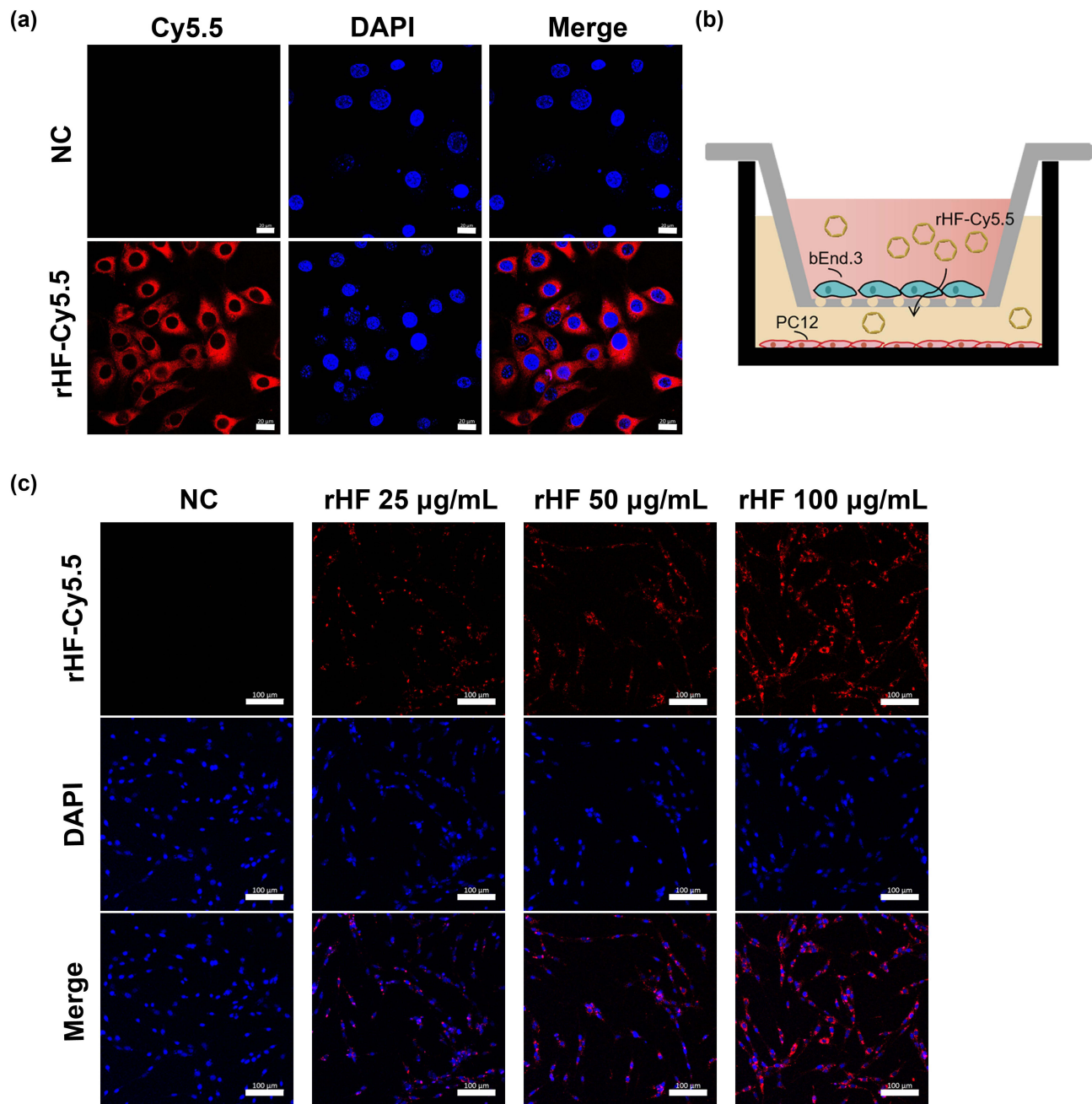


Figure 3 Permeability of rHF nanoparticles across BBB model. (a) Intracellular trafficking of Cy5.5-labeled rHF nanoparticles in bEnd.3 cells, Scale bar = 20 μm . (b) Schematic illustration of the transwell assay for constructing the BBB model in vitro. (c) Internalization of penetrative rHF nanoparticles in the lower chamber of the system with PC12 cells after transporting across BBB for 24 h, Scale bar = 100 μm .

Ferroptosis is a form of regulated cell death initiated by oxidative stress, characterized by iron-dependent accumulation of lipid peroxidation. It has been implicated in ischemia-reperfusion injury.^{35–37} Neurons respond to ferroptotic stimuli by inducing selenoproteins, such as the antioxidant GPX4.³⁵ It has been reported that ferritin protects against iron-mediated neurotoxicity and ferroptosis through mechanisms involving iron chelation.³⁸ Ferritin is also documented to inhibit hippocampal neuronal ferroptosis induced by cerebral ischemia, achieved through the downregulation of ferroptosis inducers such as p53 and SLC7A11.³⁹ To investigate the anti-ferroptosis effect of rHF, we examined the GPX4 expression in brain tissue of MCAO mice by IF. As shown in the results, ischemia-reperfusion induced the expression of GPX4 in the saline-treated group compared to the sham-operated control group. However, no increase was observed in the expression of GPX4 in the rHF-treated group

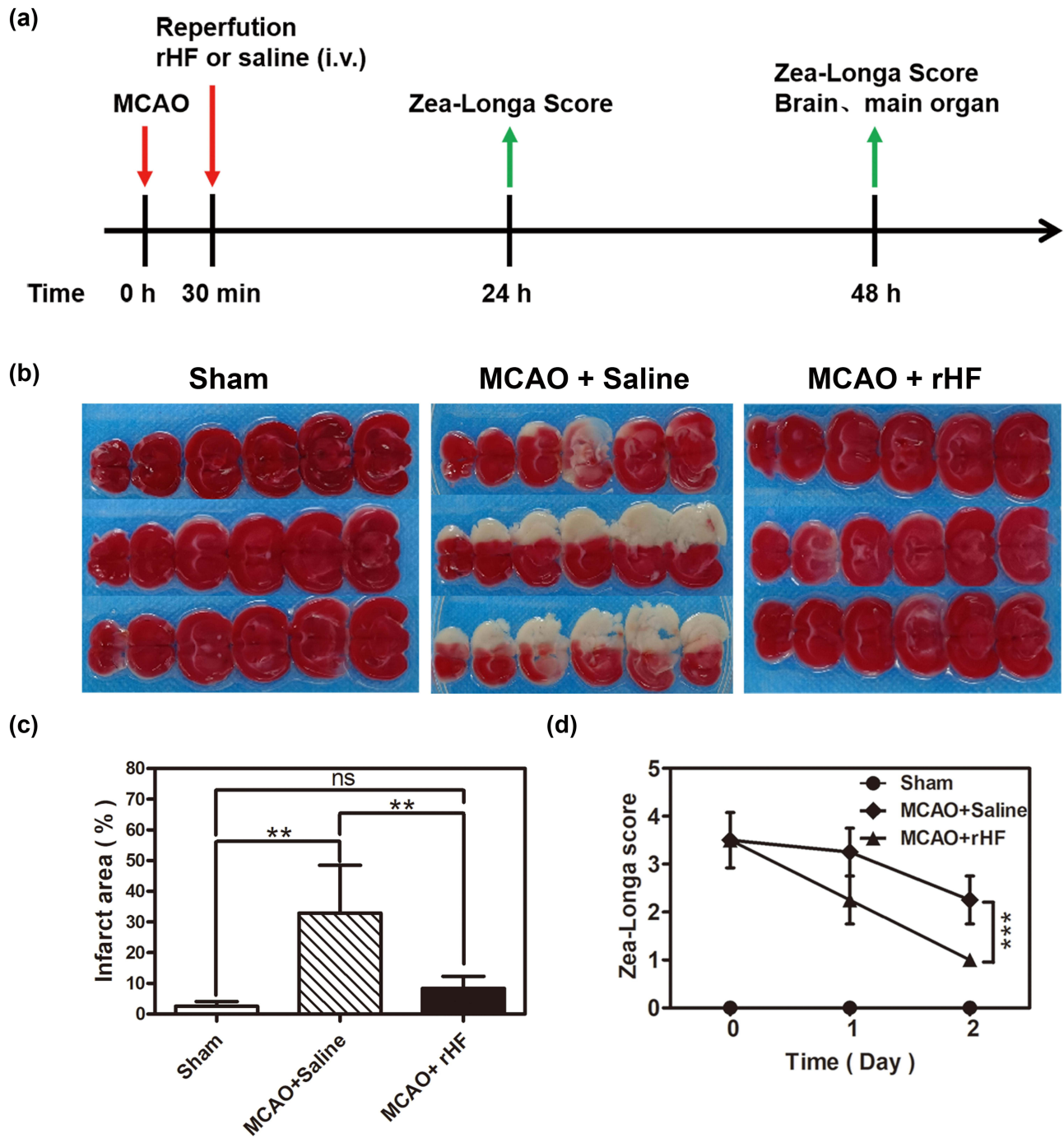


Figure 4 Therapeutic effects of rHF against ischemia-reperfusion after stroke. (a) The schedule of in vivo animal experiments. (b) Representative images of TTC-stained brain slices after treatment with rHF (30 mg/kg) for 2 days in the MCAO mice model. (c) Corresponding infarct areas of different groups were analyzed by Image ProPlus (n = 4–5). (d) Zea-Longa neurological scores of mice after different treatments for 2 days (n = 4). **P < 0.01 and ***P < 0.001.

(Figures 5c, e and S7). These findings suggest that the alleviation of cerebral ischemia-reperfusion injury by rHF may involve the inhibition of ferroptosis as one of its mechanisms.

Collectively, these results indicate that rHF effectively reduces infarct volume and mitigates neuronal damage, thereby exerting a protective effect against injuries induced by ischemia-reperfusion in stroke.

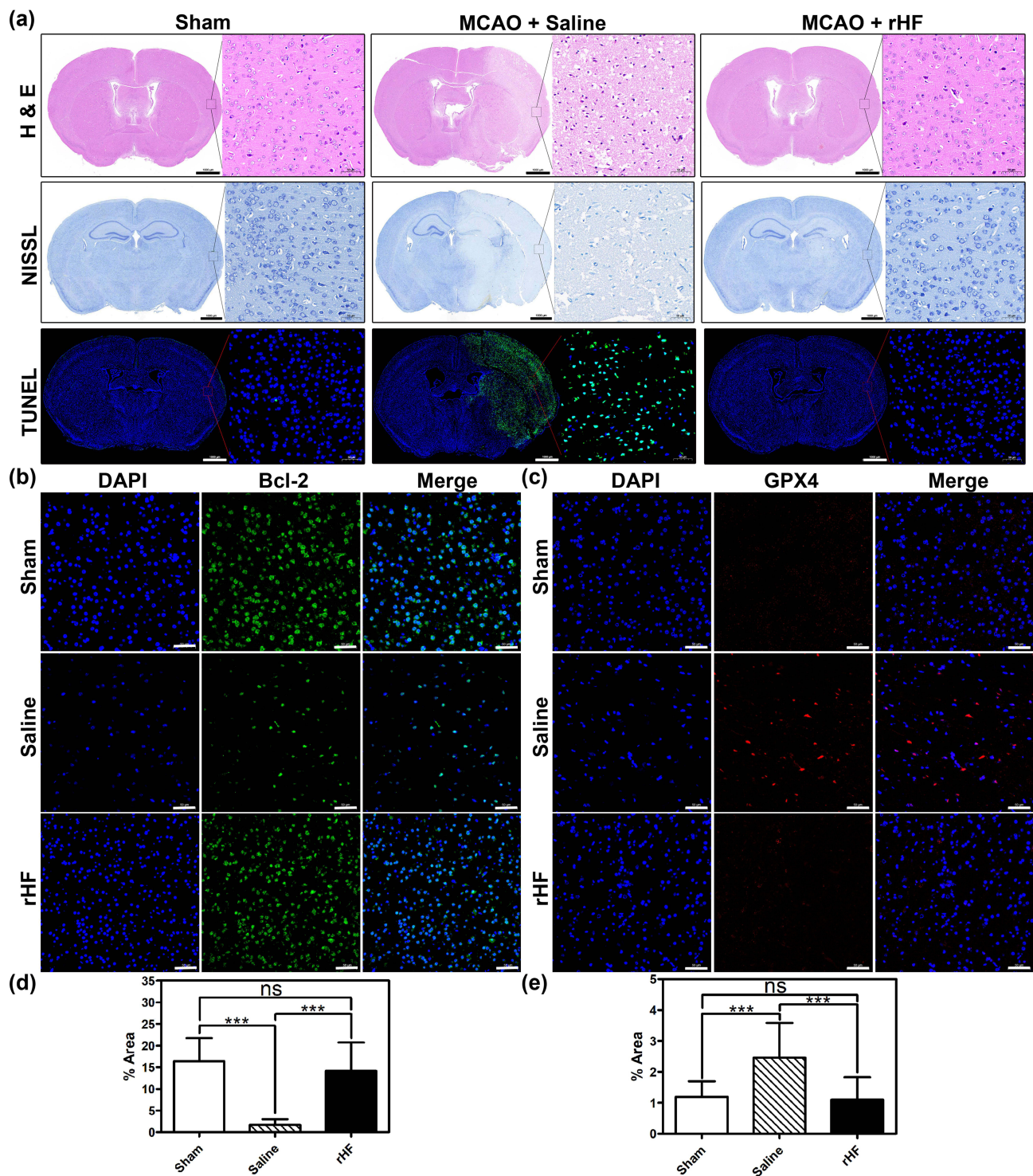


Figure 5 Evaluation of damages in the brain of MCAO mice post-treatment. **(a)** Representative photomicrographs of H&E staining, Nissl staining, and TUNEL-Hoechst costaining (Green: TUNEL; Blue: Hoechst) of brain tissues from different treatment groups. Scale bar = 1000 μ m. Bcl-2 **(b)** and GPX4 **(c)** expression in brain sections from different treatment groups examined by IF staining ($n = 3$). Scale bar = 50 μ m. The percentage of Bcl-2⁺ cell area **(d)** and GPX4⁺ cell area **(e)** in IF images analyzed with Image J ($n = 15$); *** $P < 0.001$.

rHF Suppresses Microglial Activation and HIF-1 α Expression in Ischemic Stroke

Neuroinflammation is initiated during ischemia-reperfusion injury, typically characterized by microglial activation as a hallmark feature.^{40,41} Therefore, we evaluated microglial activation based on the expression level of Iba-1 (a marker of microglia) in the brain sections of MCAO mice by IF. Compared to the sham group, the expression level of Iba-1 in

microglial cells was significantly elevated in brain sections of MCAO mice treated with saline, indicating activation of microglia in response to ischemia-reperfusion injury. After treatment with rHF (30 mg/kg) for 2 days, the expression of Iba-1 in microglia was decreased markedly (Figures 6a, c and S8). This result suggests that rHF treatment mitigates microglial activation.

HIF-1 α serves as a crucial regulator of oxygen homeostasis, with its expression rapidly upregulated following cerebral hypoxia/ischemia. HIF-1 α plays multifaceted roles in the pathophysiology of cerebral ischemia, encompassing heightened inflammation, augmented apoptosis, and compromised integrity of the BBB.^{42,43} Next, we measured the expression level of HIF-1 α in the brain sections of MCAO mice 48 h post-reperfusion via IF. The expression of HIF-1 α was significantly higher in the saline-treated group, while rHF (30 mg/kg) treatment suppressed HIF-1 α expression (Figures 6b, d and S9). These findings indicate that rHF mitigates neuroinflammation and preserves oxygen homeostasis in ischemic stroke.

Toxicity of rHF in vivo

To explore the biotoxicity of rHF in vivo, the vital organs of different treatment groups were used for histopathological analysis by H&E staining. The images of major organs (heart, liver, spleen, lung, and kidney) showed no significant pathological toxicity between the sham and treatment groups (Figure 7a). Furthermore, the concentrations of ALT, AST, urea, and creatinine in the blood of rHF-treated MCAO mice exhibited no significant alterations compared to saline-treated mice (Figure 7b–e). These results suggest that rHF did not exhibit observable in vivo toxicity.

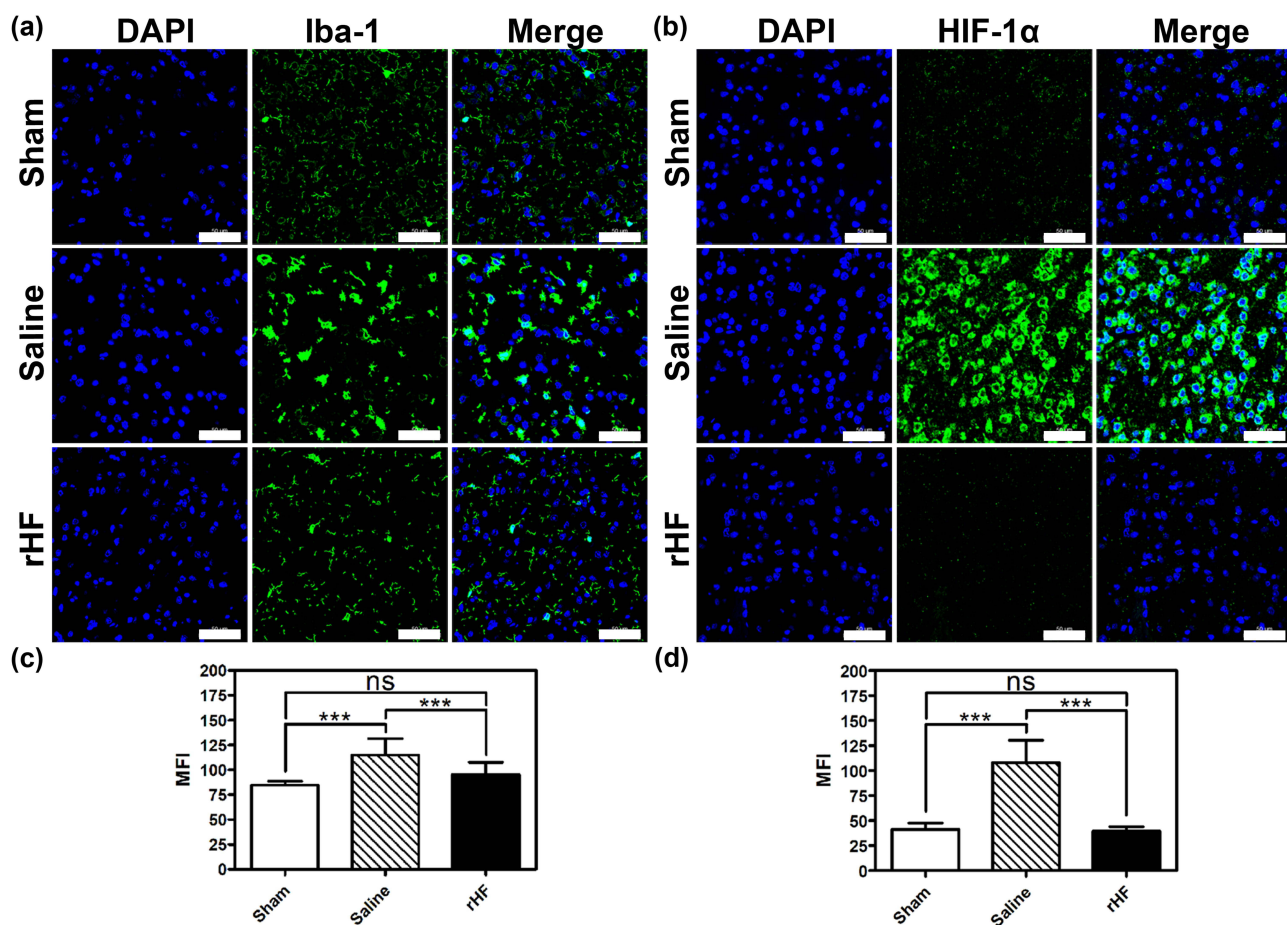


Figure 6 Microglia activation and oxygen homeostasis-related protein expression in the brain of MCAO mice after different treatments. Iba-1 (a) and HIF-1 α (b) expression in brain sections from different treatment groups examined by IF staining (n = 3). Scale bar = 50 μ m. The mean fluorescence intensity (MFI) of Iba-1⁺ cells (c) and HIF-1 α ⁺ cells (d) in IF images analyzed with Image J (n = 15); ***P < 0.001.

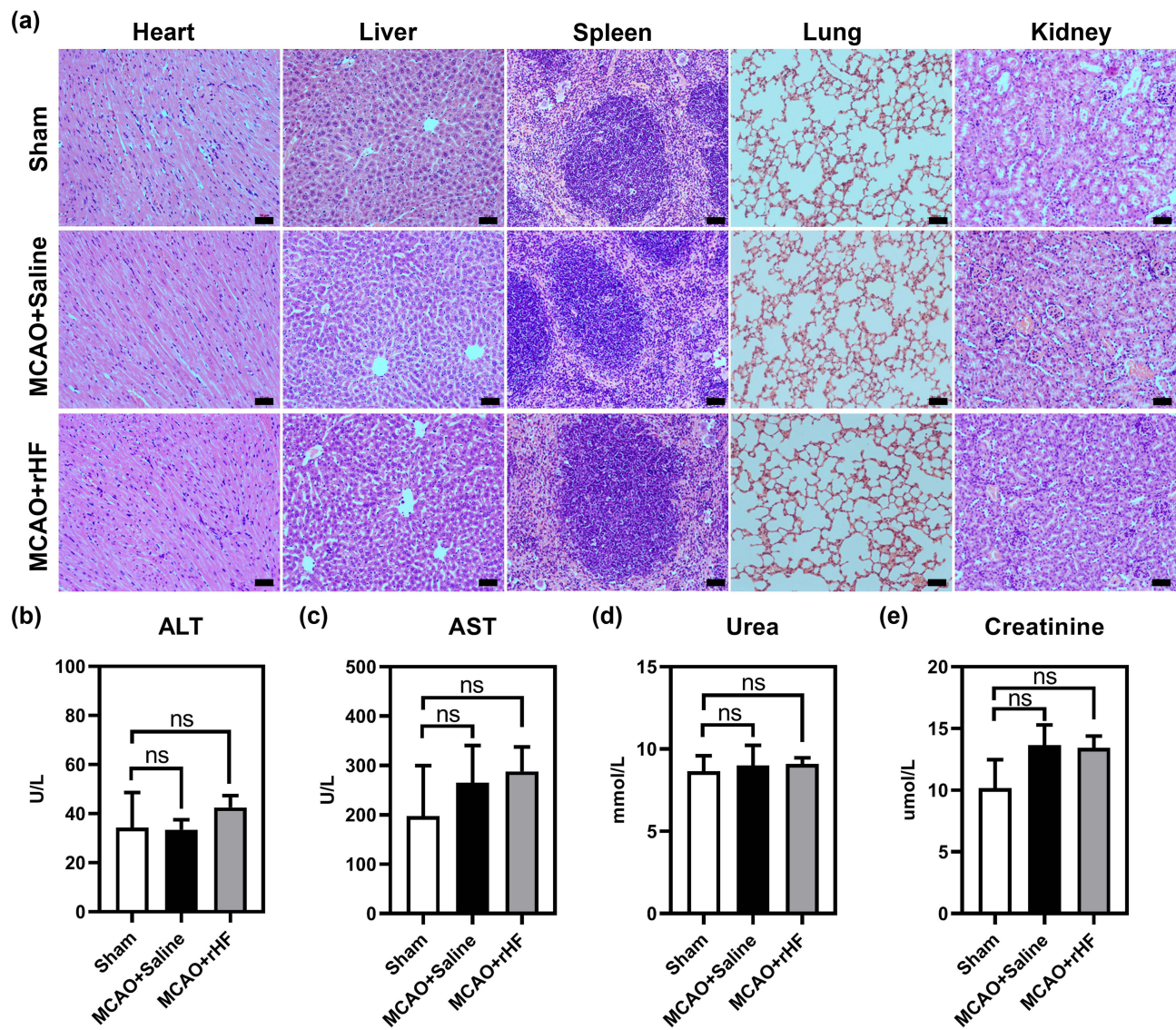


Figure 7 Biotoxicity of rHF in vivo. (a) H&E-stained tissue sections (heart, liver, spleen, lung, and kidney) from sham or MCAO mice after intravenous injections of saline or rHF (30 mg/kg), scale bar = 50 μ m. (b) The concentrations of ALT in the blood of sham or MCAO mice. (c) The concentrations of AST in the blood of sham or MCAO mice. (d) The concentrations of urea in the blood of sham or MCAO mice. (e) The concentrations of creatinine in the blood of sham or MCAO mice.

Conclusion

In summary, our findings demonstrate that rHF nanoparticles possess SOD mimetic activity, effectively eliminating excessive ROS in nerve cells and mitigating oxidative damage. Upon systemic administration, rHF nanoparticles traverse the BBB, thereby reducing oxidative damage, apoptosis, and ferroptosis of neurons while also suppressing inflammation-induced injury by inhibiting microglia activation and HIF-1 α expression in the brain tissue of MCAO model mice. These results highlight the therapeutic potential of rHF as a treatment for cerebral ischemia-reperfusion injury. Additionally, given that rHF nanoparticles serve as widely utilized drug carriers, they could be combined with other small-molecule medicines to enhance the treatment of ischemic stroke.

Ethics Statement

The animal study was reviewed and approved by the Animal Ethics Committee in the Eighth Affiliated Hospital of Sun Yat-sen University (2023-029-01).

Acknowledgments

This work was supported by Futian Healthcare Research Project (No. FTWS2023061) and the National Natural Science Foundation of China (No. 81903146).

Disclosure

The authors report no conflicts of interest in this work.

References

1. Feigin VL, Brainin M, Norrving B, et al. World Stroke Organization (WSO): global stroke fact sheet 2022. *Int J Stroke*. 2022;17(1):18–29. doi:10.1177/17474930211065917
2. Hankey GJ. Stroke. *Lancet*. 2017;389(10069):641–654. doi:10.1016/S0140-6736(16)30962-X
3. Paul S, Candelario-Jalil E. Emerging neuroprotective strategies for the treatment of ischemic stroke: an overview of clinical and preclinical studies. *Exp Neurol*. 2021;335:113518. doi:10.1016/j.expneurol.2020.113518
4. Feske SK. Ischemic stroke. *Am J Med*. 2021;134(12):1457–1464. doi:10.1016/j.amjmed.2021.07.027
5. Powers WJ. Acute ischemic stroke. *N Engl J Med*. 2020;383(3):252–260. doi:10.1056/NEJMcp1917030
6. Lo EH, Moskowitz MA, Jacobs TP. Exciting, radical, suicidal: how brain cells die after stroke. *Stroke*. 2005;36(2):189–192. doi:10.1161/01.STR.0000153069.96296.fd
7. Zhao Y, Zhang X, Chen X, Wei Y. Neuronal injuries in cerebral infarction and ischemic stroke: from mechanisms to treatment (review). *Int J Mol Med*. 2022;49(2):1–9.
8. Orellana-Urzua S, Rojas I, Libano L, Rodrigo R. Pathophysiology of ischemic stroke: role of oxidative stress. *Curr Pharm Des*. 2020;26(34):4246–4260. doi:10.2174/1381612826666200708133912
9. Higashi Y. Edaravone for the treatment of acute cerebral infarction: role of endothelium-derived nitric oxide and oxidative stress. *Expert Opin Pharmacother*. 2009;10(2):323–331. doi:10.1517/14656560802636888
10. Liu X, Ma Y, Wang Y, Zhang Q. Effects of NBP injection on the inflammatory response, oxidative stress response and vascular endothelial function in patients with ACI: a systematic review and meta-analysis. *Medicine*. 2023;102(10):e33226. doi:10.1097/MD.00000000000033226
11. Amarenco P, Bogousslavsky J, Callahan A, et al. High-dose atorvastatin after stroke or transient ischemic attack. *N Engl J Med*. 2006;355(6):549–559.
12. Bao Q, Hu P, Xu Y, et al. Simultaneous blood-brain barrier crossing and protection for stroke treatment based on edaravone-loaded ceria nanoparticles. *ACS Nano*. 2018;12(7):6794–6805. doi:10.1021/acsnano.8b01994
13. He L, Huang G, Liu H, Sang C, Liu X, Chen T. Highly bioactive zeolitic imidazolate framework-8-capped nanotherapeutics for efficient reversal of reperfusion-induced injury in ischemic stroke. *Sci Adv*. 2020;6(12):eaay9751. doi:10.1126/sciadv.aay9751
14. Ni D, Wei H, Chen W, et al. Ceria nanoparticles meet hepatic ischemia-reperfusion injury: the perfect imperfection. *Adv Mater*. 2019;31(40):e1902956. doi:10.1002/adma.201902956
15. Liu Y, Ai K, Ji X, et al. Comprehensive insights into the multi-antioxidative mechanisms of melanin nanoparticles and their application to protect brain from injury in ischemic stroke. *J Am Chem Soc*. 2017;139(2):856–862. doi:10.1021/jacs.6b11013
16. Niu Y, Tan H, Li X, et al. Protein-carbon dot nanohybrid-based early blood-brain barrier damage theranostics. *ACS Appl Mater Interfaces*. 2020;12(3):3445–3452. doi:10.1021/acsnano.1b19378
17. Takamiya M, Miyamoto Y, Yamashita T, Deguchi K, Ohta Y, Abe K. Strong neuroprotection with a novel platinum nanoparticle against ischemic stroke- and tissue plasminogen activator-related brain damages in mice. *Neuroscience*. 2012;221:47–55. doi:10.1016/j.neuroscience.2012.06.060
18. Li C, Zhao Z, Luo Y, et al. Macrophage-disguised manganese dioxide nanoparticles for neuroprotection by reducing oxidative stress and modulating inflammatory microenvironment in acute ischemic stroke. *Adv Sci*. 2021;8(20):e2101526. doi:10.1002/advs.202101526
19. Wang Z, Zhao Y, Hou Y, et al. A thrombin-activated peptide-templated nanozyme for remedying ischemic stroke via thrombolytic and neuroprotective actions. *Adv Mater*;2023. e2210144. doi:10.1002/adma.202210144
20. Li Y, Cui R, Fan F, et al. The efficacy and safety of ischemic stroke therapies: an umbrella review. *Front Pharmacol*. 2022;13:924747. doi:10.3389/fphar.2022.924747
21. Li K, Zhang ZP, Luo M, et al. Multifunctional ferritin cage nanostructures for fluorescence and MR imaging of tumor cells. *Nanoscale*. 2012;4(1):188–193. doi:10.1039/C1NR11132A
22. Bhushan B, Kumar SU, Matai I, Sachdev A, Dubey P, Gopinath P. Ferritin nanocages: a novel platform for biomedical applications. *J Biomed Nanotechnol*. 2014;10(10):2950–2976. doi:10.1166/jbn.2014.1980
23. Inoue I, Chiba M, Ito K, et al. One-step construction of ferritin encapsulation drugs for cancer chemotherapy. *Nanoscale*. 2021;13(3):1875–1883. doi:10.1039/D0NR04019C
24. Liu D, Ji Q, Cheng Y, et al. Cyclosporine A loaded brain targeting nanoparticle to treat cerebral ischemia/reperfusion injury in mice. *J Nanobiotechnology*. 2022;20(1):256. doi:10.1186/s12951-022-01474-x
25. Zhao S, Duan H, Yang Y, Yan X, Fan K. fenozyme protects the integrity of the blood-brain barrier against experimental cerebral malaria. *Nano Lett*. 2019;19(12):8887–8895. doi:10.1021/acsnanolett.9b03774
26. Fan K, Jia X, Zhou M, et al. Ferritin nanocarrier traverses the blood brain barrier and kills glioma. *ACS Nano*. 2018;12(5):4105–4115. doi:10.1021/acsnano.7b06969
27. Wang L, Zhang B, Yang X, et al. Targeted alleviation of ischemic stroke reperfusion via atorvastatin-ferritin Gd-layered double hydroxide. *Bioact Mater*. 2023;20:126–136. doi:10.1016/j.bioactmat.2022.05.012
28. Pham CG, Bubicic C, Zazzeroni F, et al. Ferritin heavy chain upregulation by NF-kappaB inhibits TNFalpha-induced apoptosis by suppressing reactive oxygen species. *Cell*. 2004;119(4):529–542. doi:10.1016/j.cell.2004.10.017
29. Park E, Chung SW. ROS-mediated autophagy increases intracellular iron levels and ferroptosis by ferritin and transferrin receptor regulation. *Cell Death Dis*. 2019;10(11):822. doi:10.1038/s41419-019-2064-5

30. Yuan X, Cong Y, Hao J, et al. Regulation of LIP level and ROS formation through interaction of H-ferritin with G-CSF receptor. *J Mol Biol.* 2004;339(1):131–144. doi:10.1016/j.jmb.2004.03.027
31. Wang Y, Branicky R, Noe A, Hekimi S. Superoxide dismutases: dual roles in controlling ROS damage and regulating ROS signaling. *J Cell Biol.* 2018;217(6):1915–1928. doi:10.1083/jcb.201708007
32. Arosio P, Levi S. Ferritin, iron homeostasis, and oxidative damage. *Free Radic Biol Med.* 2002;33(4):457–463. doi:10.1016/S0891-5849(02)00842-0
33. Torti FM, Torti SV. Regulation of ferritin genes and protein. *Blood.* 2002;99(10):3505–3516. doi:10.1182/blood.V99.10.3505
34. Jiang X, Andjelkovic AV, Zhu L, et al. Blood-brain barrier dysfunction and recovery after ischemic stroke. *Prog Neurobiol.* 2018;163-164:144–171. doi:10.1016/j.pneurobio.2017.10.001
35. Alim I, Caulfield JT, Chen Y, et al. Selenium drives a transcriptional adaptive program to block ferroptosis and treat stroke. *Cell.* 2019;177(5):1262–1279. doi:10.1016/j.cell.2019.03.032
36. Xu Y, Li K, Zhao Y, Zhou L, Liu Y, Zhao J. Role of ferroptosis in stroke. *Cell Mol Neurobiol.* 2023;43(1):205–222. doi:10.1007/s10571-022-01196-6
37. Pan Y, Wang X, Liu X, Shen L, Chen Q, Shu Q. Targeting ferroptosis as a promising therapeutic strategy for ischemia-reperfusion injury. *Antioxidants.* 2022;11(11):2196. doi:10.3390/antiox11112196
38. Zhang N, Yu X, Song L, Xiao Z, Xie J, Xu H. Ferritin confers protection against iron-mediated neurotoxicity and ferroptosis through iron chelating mechanisms in MPP(+)-induced MES23.5 dopaminergic cells. *Free Radic Biol Med.* 2022;193:751–763. doi:10.1016/j.freeradbiomed.2022.11.018
39. Chen W, Jiang L, Hu Y, et al. Ferritin reduction is essential for cerebral ischemia-induced hippocampal neuronal death through p53/SLC7A11-mediated ferroptosis. *Brain Res.* 2021;1752:147216. doi:10.1016/j.brainres.2020.147216
40. Xiong XY, Liu L, Yang QW. Functions and mechanisms of microglia/macrophages in neuroinflammation and neurogenesis after stroke. *Prog Neurobiol.* 2016;142:23–44. doi:10.1016/j.pneurobio.2016.05.001
41. Xu P, Zhang X, Liu Q, et al. Microglial TREM-1 receptor mediates neuroinflammatory injury via interaction with SYK in experimental ischemic stroke. *Cell Death Dis.* 2019;10(8):555.
42. He Q, Ma Y, Liu J, et al. Biological functions and regulatory mechanisms of hypoxia-inducible factor-1alpha in ischemic stroke. *Front Immunol.* 2021;12:801985. doi:10.3389/fimmu.2021.801985
43. Jiang Q, Geng X, Warren J, et al. Hypoxia Inducible Factor-1alpha (HIF-1alpha) mediates NLRP3 inflammasome-dependent-pyrototic and apoptotic cell death following ischemic stroke. *Neuroscience.* 2020;448:126–139. doi:10.1016/j.neuroscience.2020.09.036

International Journal of Nanomedicine

Dovepress

Publish your work in this journal

The International Journal of Nanomedicine is an international, peer-reviewed journal focusing on the application of nanotechnology in diagnostics, therapeutics, and drug delivery systems throughout the biomedical field. This journal is indexed on PubMed Central, MedLine, CAS, SciSearch®, Current Contents®/Clinical Medicine, Journal Citation Reports/Science Edition, EMBase, Scopus and the Elsevier Bibliographic databases. The manuscript management system is completely online and includes a very quick and fair peer-review system, which is all easy to use. Visit <http://www.dovepress.com/testimonials.php> to read real quotes from published authors.

Submit your manuscript here: <https://www.dovepress.com/international-journal-of-nanomedicine-journal>